Hyperfine Interact (2016) 237: 131
DOI 10.1007/s10751-016-1335-0

Indium-defect interactions in FCC and BCC metals studied using the modified embedded atom method

M. O. Zacate[1]

Published online: 27 September 2016
© Springer International Publishing Switzerland 2016

Abstract With the aim of developing a transferable potential set capable of predicting defect formation, defect association, and diffusion properties in a wide range of intermetallic compounds, the present study was undertaken to test parameterization strategies for determining empirical pair-wise interaction parameters in the modified embedded atom method (MEAM) developed by Baskes and coworkers. This report focuses on indium-solute and indium-vacancy interactions in FCC and BCC metals, for which a large set of experimental data obtained from perturbed angular correlation measurements is available for comparison. Simulation results were found to be in good agreement with experimental values after model parameters had been adjusted to reproduce as best as possible the following two sets of quantities: (1) lattice parameters, formation enthalpies, and bulk moduli of hypothetical equiatomic compounds with the NaCl crystal structure determined using density functional theory and (2) dilute solution enthalpies in metals as predicted by Miedema's semi-empirical model.

Keywords MEAM · Point defect · Defect association

1 Introduction

Perturbed angular correlation spectroscopy (PAC) and other hyperfine methods can be used to study movement of tracer atoms in materials through measurement of nuclear relaxation. Because these methods are sensitive to changes near tracers at the atomic scale, they have

This article is part of the Topical Collection on *Proceedings of the International Conference on Hyperfine Interactions and their Applications (HYPERFINE 2016), Leuven, Belgium, 3-8 July 2016*

✉ M. O. Zacate
zacatem1@nku.edu

[1] Department of Physics, Geology, and Engineering Technology, Northern Kentucky University, Highland Heights, KY 41099, USA

the potential to help elucidate operative diffusion mechanisms in intermetallic compounds, especially when defects involved in the diffusion mechanism are attracted to the tracers. In-111 PAC has been applied to study cadmium movement in a wide range of intermetallic compounds, but so far it has not been possible to simultaneously observe nuclear relaxation due to tracer movement and bound defects [1–11]. It appears that such a situation is uncommon, and it is therefore desirable to have tools available to make meaningful predictions about which combinations of PAC tracers and binary intermetallic compounds are likely to yield PAC spectra that exhibit both defect-induced signals and relaxation.

The long-term goal of this work is to apply computer simulations to predict solute site occupation, defect formation, defect association, and defect migration enthalpies for PAC tracers in a broad range of intermetallic compounds. To be successful, a reliable yet quick simulation method is required. While calculations based on density functional theory (DFT) are reliable, they are computationally demanding. The modified embedded atom method (MEAM), [12] on the other hand, is a semi-empirical simulation method that does not require as much computing time. It has proven reliable for predicting a number of materials properties, including defect properties, of 22 pure metals [12–20]. Its use to simulate binary alloys has been more limited, but results are promising [21–28]. The aim of the present work is to introduce a slight modification to the scheme typically used to parameterize the empirical potentials used in the MEAM technique. Its reliability is reported here by comparing calculated indium-defect binding enthalpies in FCC and BCC metals to values obtained from experiment [29–37].

2 Methodology

In the modified embedded atom method, empirical parameters needed for the pure elements are determined by adjusting model parameters until typically 14 or more different experimentally measured properties are reproduced. For an alloy, there are fewer empirical parameters in the pair-wise interaction than there are for the metals, so usually fewer properties are tested in the development of potentials for alloys. For an alloy, the primary properties evaluated are the formation enthalpy, lattice parameter, and elastic properties of a reference structure, often compared to those values determined from experiment if the reference structure exists in nature or alternatively to values obtained from higher level calculations [27].

In this work, some of the element-pairs do not form stable intermetallic phases, so empirical parameters cannot be determined by comparison to experimentally determined quantities. Following the work of Jelinek et al. [22], a hypothetical reference structure was used for equiatomic compositions, the NaCl structure, with alloy properties predicted using density functional theory (DFT). For consistency, the same procedure was used even for those element pairs that do form stable intermetallic phases. Formation enthalpy, lattice parameter, and bulk modulus of the reference structure can be reproduced exactly for a variety of choices for model parameters; however, the elastic constants typically cannot be reproduced exactly for any choice (for example, as discussed in Ref. [22]). Therefore, other observables are needed to tie down the model parameters for the alloys.

One option is to use relative formation enthalpies of polymorphs of a selection of alloy compositions determined using DFT [22]. In anticipation of applying MEAM calculations to a large set of alloys, an alternative approach that minimizes the number of required DFT calculations was tested in the present work. Here, model parameters were determined

by calculating dilute solution enthalpies and comparing them to values calculated using the semi-empirical Miedema model. Details of the MEAM model, DFT calculations, and Miedema model are given below.

2.1 Modified embedded atom method

In the embedded atom method (EAM), the total energy of a material is given by

$$E_{\text{total}} = \sum_i F_i(\bar{\rho}_i) + \frac{1}{2}\sum_{j\neq i}\phi_{ij}(r_{ij}) \tag{1}$$

where i and j are summation indexes over atoms in the simulation space, F_i is the embedding function for atom i, $\bar{\rho}_i$ is the background electron density at the site atom i occupies, and $\phi(r_{ij})$ is the short range pair interaction between atoms i and j when separated by distance r_{ij} [38, 39]. The functional forms of F_i, $\bar{\rho}_i$, and ϕ_{ij} vary substantially among different implementations of the EAM. The present work uses the variation first introduced by Baskes [12], called the modified embedded atom method (MEAM). Even this variation has evolved over the years, so to be clear, exact forms of various functions used in the present work are provided in the Appendix.

For simulation of a metal composed of a single element, the model requires 17 parameters, including cutoff parameters, to specify $\bar{\rho}_i$ and $\phi_{ij}(r_{ij})$ completely. These have been determined already for the elements considered in this work [13–15, 20]. For alloys, additional parameters are needed for each pair of elements and for ternary combinations. Each element has one additional parameter – the density scaling parameter ρ_0 – that does not affect calculated properties of single-element metals but serves as one additional adjustable parameter for alloys.

Following the work of Jelinek et al. [22], the short range potential for an alloy is expressed in terms of the cohesive energy E_c – defined with respect to neutral atoms at infinity, nearest neighbor distance r_{1e}, and dimensionless quantity α of a compound with the NaCl structure formed by the pair of elements in the alloy. This leaves the d-parameter from Rose's universal equation of state and the short-range potential cutoff distance as the final parameters needed for the short range potential. There are 10 more parameters needed for screening: the cutoff separation r_c, the taper range Δr, and the angular bounding parameters $C_{\min}^{ABA}$, $C_{\min}^{BAB}$, $C_{\min}^{AAB} = C_{\min}^{BAA}$, $C_{\min}^{ABB} = C_{\min}^{BBA}$, $C_{\max}^{ABA}$, $C_{\max}^{BAB}$, $C_{\max}^{AAB} = C_{\max}^{BAA}$ and $C_{\max}^{ABB} = C_{\max}^{BBA}$. Additional bounding parameters for screening are needed when three different elements are involved. These are $C_{\min}^{BAC} = C_{\min}^{CAB}$, $C_{\min}^{CBA} = C_{\min}^{ABC}$, and $C_{\min}^{ACB} = C_{\min}^{BCA}$, $C_{\max}^{BAC} = C_{\max}^{CAB}$, $C_{\max}^{CBA} = C_{\max}^{ABC}$, and $C_{\max}^{ACB} = C_{\max}^{BCA}$.

In this work, all $C_{\max}$ values were taken to be 2.80, and 0.10 Å was used for the taper range of all screening functions. The screening cutoff separation for element pairs was taken to be the DFT-predicted lattice parameter of the NaCl structure, rounded to the nearest 0.1 Å. The cutoff range of all short range pair potentials was taken to be 8.0 Å. The remaining parameters were chosen to reproduce the formation enthalpy, lattice parameter, and bulk modulus of the NaCl-structured compounds predicted by DFT and the dilute solution enthalpies predicted by the Miedema model as best as possible.

As a starting point in the search for an optimal parameter set, cohesive enthalpies and nearest neighbor distances were constrained to those values predicted by DFT and the d-parameter held at the commonly used value of 0.05. In addition, default bounding parameters based on the pure elements were used as follows: $C_{\min}^{ABA} = C_{\min}^{AAA}$, $C_{\min}^{BAB} =$

$C_{\min}^{BBB}$, $C_{\min}^{ABB} = C_{\min}^{AAB} = \left(\frac{1}{2}\sqrt{C_{\min}^{AAA}} + \frac{1}{2}\sqrt{C_{\min}^{BBB}}\right)$, $C_{\min}^{ABC} = \left(\frac{1}{2}\sqrt{C_{\min}^{AAA}} + \frac{1}{2}\sqrt{C_{\min}^{CCC}}\right)$, $C_{\min}^{BCA} = \left(\frac{1}{2}\sqrt{C_{\min}^{BBB}} + \frac{1}{2}\sqrt{C_{\min}^{AAA}}\right)$, and $C_{\min}^{CAB} = \left(\frac{1}{2}\sqrt{C_{\min}^{CCC}} + \frac{1}{2}\sqrt{C_{\min}^{BBB}}\right)$. Under these conditions, the density scaling factors of pure elements and α-parameters of the alloys were adjusted until the target parameters were crudely optimized. After that, the density scaling factors were held fixed while the cohesive energy, first neighbor distances and α-parameters of individual alloys were adjusted. If the target parameters were not reproduced satisfactorily, then the pair-wise angular-bounding parameters and d-parameters were adjusted also.

MEAM calculations were carried out using an early-release-version 4.3 of the General Utility Lattice Program (GULP) [40, 41]. Calculations of dilute solution enthalpies were performed by substituting a host element with one solute atom in structure-dependent sized supercells: 3× 3× 3 for FCC, 4× 4× 4 for BCC, 4× 4× 3 for the body-centered tetragonal In, and 3× 2× 3 for the oC8-structured Ga. Defect enthalpies for calculation of In-defect binding were carried out in 6× 6× 6 supercells for both the FCC and the BCC structured metals. Unit cell, supercell lattice parameters, and atomic coordinates were allowed to relax fully in all calculations.

2.2 Density functional theory

Properties of hypothetical NaCl-structured compounds were calculated using the projector augmented-wave method [42, 43] implemented in the VASP code [44, 45]. Exchange-correlation effects were treated by the generalized gradient approximation of Perdew et al. [46]. All calculations were performed in high precision with the plane-wave cutoff energies set to 1.5 times the larger default PAW cutoff energy of each element pair. Integration was performed using the Γ-centered Monkhorst-Pack scheme [47] of size 22× 22× 22. Bulk moduli were calculated by fitting enthalpy-volume dependence to the Birch-Murnaghan equation of state [48].

2.3 Miedema model

With the aim of minimizing the number of computationally demanding DFT calculations, dilute solution enthalpies were calculating using the Miedema semi-empirical model [49, 50]. Within this model, calculations depend on the following bulk metal properties of each element under consideration: the work function ϕ; the electronic density at the Wigner-Seitz cell boundary, n_{ws}; the atomic volume V; the bulk modulus K; and the shear modulus G. The values for these parameters as tabulated in Ref. [50] were used in this work.

The enthalpy of dilute solution is the sum of a chemical contribution and an elastic contribution: $H_{\mathrm{sol}}\,(B\mathrm{in}A) = H_{\mathrm{chem}}\,(B\mathrm{in}A) + H_{\mathrm{elastic}}\,(B\mathrm{in}A)$. Calculation of the chemical contribution is based on the premise that there is a characteristic interfacial energy between elements of type A and B, given by

$$\Delta h_{A,B}^{\mathrm{inter}} = \frac{2}{\left((n_{ws})_A^{-1/3} + (n_{ws})_B^{-1/3}\right)} \left\{-P\,(\phi_A - \phi_B)^2 + Q\left((n_{ws})_A^{1/3} - (n_{ws})_B^{1/3}\right)^2 - R\right\} \tag{2}$$

where P, Q, and R, are empirical parameters that depend on the valences of elements A and B. The values put forth in Ref. [49] for the solid phase are used in the present work. The chemical enthalpy is found by multiplying the interfacial term by a contact area:

Table 1 References to work that derived the single-element MEAM parameters and values of density scaling factors ρ_0 used in the present work

Element	Reference	ρ_0
Ag	[14]	0.89
Al	[14]	0.88
Au	[14]	1.08
Cu	[14]	1.31
Ga	[15]	0.99
In	[20]	1.00
Mo	[13]	1.14
Nb	[13]	1.07
Ni	[14]	2.26
Pd	[14]	1.29
Pt	[14]	0.89
Ta	[13]	1.22
W	[13]	1.43

$H_{\text{chem}}\,(A\text{in}B) = \Omega_A^{2/3}\,\Delta h_{A,B}^{\text{inter}}$ where $\Omega_A^{2/3} = V_A^{2/3}\,[1 + a\,(\phi_A - \phi_B)]$ accounts for a change in atomic size when atom A is surrounded by atoms of type B. Here, a is yet another empirical parameter that depends on the valences of A and B with values selected from Ref. [49].

The elastic contribution is motivated by the classical problem of filling a spherical hole in one material with a sphere made of another material [51]. This leads to the equation

$$H_{\text{elastic}}\,(A\text{in}B) = \frac{2K_A G_B\,(W_B - W_A)^2}{3K_A W_B + 4G_B W_A} \tag{3}$$

where W_A and W_B are the volumes of the elements upon alloying. These volumes are given by $W_A = V_A + \alpha\,(\phi_B - \phi_A)\,/\,(n_{ws})_A$ and $W_B = V_B + \alpha(\phi_B - \phi_A)/(n_{ws})_B$ with $\alpha = -3\Omega_A^{2/3}/2/\left((n_{ws})_A^{-1/3} + (n_{ws})_A^{-1/3}\right)$.

3 Results and discussion

The MEAM model parameters derived using the method described in Section 2 are given in Tables 1, 2 and 3. A summary of how well simulations using these parameters reproduce the target parameters of the NaCl-structured compound – formation enthalpy H_{form}, lattice parameter a, and bulk modulus B – using DFT and solution enthalpies calculated using the Miedema model is given in Table 4. Experimental values for available solution enthalpies [52] are also given in Table 4. As can be seen, it was not possible to get perfect agreement with all the target parameters. Final values for model parameters were chosen so that deviations between calculated and target values throughout the entire set were balanced approximately equally among physical quantities. That is, care was given to avoid biasing the potential set to reproducing alloy formation enthalpy or lattice parameter, as examples. Ranges in the deviations of H_{form} and a for the NaCl structure are of the same order as in Jelinek et al. [22], whereas deviations in bulk moduli were larger in the present work. The larger deviation was often necessary to obtain acceptable values for solution enthalpies, which Jelinek et al. did not consider.

Table 2 Binary alloy MEAM parameters derived for the present study

A-B	E_c (eV)	r_{1e} (Å)	α	d	C_{min}^{BAB}	C_{min}^{ABA}	C_{min}^{AAB}	C_{min}^{ABB}	r_c (Å)
Ag-Au	3.115	2.666	5.36497	0.000	1.53	1.38	1.45	1.45	5.5
Ag-Cu	2.801	2.524	5.25420	0.050	1.21	1.38	1.29	1.29	5.2
Ag-In	2.654	2.796	5.44650	0.000	1.50	1.38	1.44	1.44	5.8
Ag-Pd	2.973	2.665	5.50931	0.000	1.69	1.38	1.53	1.53	5.4
Ag-Pt	3.754	2.654	5.60475	0.000	1.53	1.38	1.45	1.45	5.4
Au-In	3.382	2.805	5.24695	0.000	1.50	1.53	1.51	1.51	5.7
Au-Pd	3.524	2.646	5.71997	0.000	1.69	1.53	1.61	1.61	5.4
Au-Pt	4.362	2.600	5.75573	0.050	1.53	1.53	1.53	1.53	5.4
Cu-In	2.853	2.722	5.76794	0.085	1.50	1.21	0.31	0.52	5.5
Cu-Pd	3.357	2.493	5.38365	0.000	1.69	1.21	1.44	1.44	5.0
Cu-Pt	4.262	2.486	5.40415	0.000	1.53	1.21	1.37	1.37	5.0
In-Pd	3.599	2.724	5.30896	0.050	1.69	1.50	1.59	1.59	5.5
In-Pt	4.420	2.738	5.34237	0.050	1.53	1.50	1.51	1.51	5.5
Ag-Ga	2.844	2.619	5.03310	0.000	1.40	1.38	1.39	1.39	5.5
Ga-In	2.629	2.804	6.43061	0.050	0.90	1.00	0.95	0.95	5.8
Al-In	2.780	2.871	5.10314	0.050	1.50	0.49	0.93	0.93	5.8
In-Mo	3.400	2.840	6.20592	0.050	0.64	1.50	1.02	1.02	5.5
In-Nb	4.294	2.897	5.28615	0.050	0.36	1.50	0.83	0.83	5.6
In-Ni	3.524	2.579	5.32343	0.198	0.05	0.15	0.02	0.03	5.2
In-Ta	4.357	2.938	5.35327	0.000	0.25	1.50	0.74	0.74	5.6
In-W	3.830	2.880	6.08976	0.050	0.49	1.50	0.93	0.93	5.5

Table 3 MEAM parameters for the ternary alloys

A-B-C	$C_{min}^{BAC} = C_{min}^{CAB}$	$C_{min}^{CBA} = C_{min}^{ABC}$	$C_{min}^{ACB} = C_{min}^{BCA}$
In-Ag-Au	1.51	1.44	1.45
In-Ag-Cu	1.35	1.44	1.29
In-Ag-Ga	1.45	1.44	1.39
In-Ag-Pd	1.59	1.44	1.53
In-Ag-Pt	1.51	1.44	1.45
In-Au-Pd	1.59	1.51	1.61
In-Au-Pt	1.51	1.51	1.53
In-Cu-Pd	1.59	1.35	1.44
In-Cu-Pt	1.51	1.35	1.37

Binding enthalpies between indium solutes and other substitutional solutes or vacancies in selected FCC and BCC compounds were calculated by taking the difference in supercell enthalpies with the indium and defect in first-neighbor positions and supercell enthalpies with isolated defects. Results of the MEAM calculations along with values from experiment, where available, are listed in Tables 5 and 6. As can be seen, MEAM values and experimental values generally agree within 0.1 eV with many deviations even smaller than that. There are two notable exceptions: the In-vacancy binding enthalpies in Cu and W.

Table 4 Comparison of MEAM-calculated quantities (top row for each element pair) and DFT-calculated ΔH_{form}, a, and B and solution enthalpies calculated using the Miedema model. Experimental values of solution enthalpies from ref. [52], if available, are shown in italics

A-B	ΔH_{form} (eV/AB)	a (A)	B (GPa)	$H_{\text{sol}}(B \text{ in } A)$	$H_{\text{sol}}(A \text{ in } B)$
Ag-Au	0.530	5.3320	84.2	−0.23	−0.23
	0.468	5.5050	80.3	−0.24 *−0.19*	−0.21 *−0.16*
Ag-Cu	0.838	5.0480	85.6	0.21	0.40
	0.874	5.1614	81.2	0.24 *0.25*	0.33 *0.39*
Ag-Ga	0.073	5.2380	72.1	3.21	−0.30
	0.322	5.4547	55.5	−0.26 *−0.16*	−0.23 *0.02*
Ag-In	0.162	5.5920	64.1	0.06	−0.03
	0.246	5.7958	46.7	0.12	−0.06
Ag-Pd	0.894	5.3300	84.9	−0.35	−0.18
	0.930	5.3719	85.1	−0.30 *−0.29*	−0.29 *−0.11*
Ag-Pt	1.282	5.3080	112.3	−0.05	0.03
	1.304	5.3535	112.4	−0.04	−0.03
Al-In	0.466	5.7722	52.6	0.67	0.26
	0.638	5.8280	42.5	0.60	0.31
Au-In	−0.434	5.6100	75.1	−0.48	−0.57
	−0.382	5.7480	62.6	−0.23 *−0.62*	−0.48 *−0.49*
Au-Pd	0.652	5.2920	110.8	−0.07	0.15
	0.622	5.3612	110.5	0.03 *−0.36*	0.05 *−0.20*
Au-Pt	0.926	5.2000	146.4	0.15	0.22
	0.898	5.3564	143.8	0.19	0.21
Cu-In	0.306	5.4438	64.2	1.07	0.13
	0.476	5.4643	58.3	0.80	0.11
Cu-Pd	0.666	4.9860	111.8	−0.28	−0.41
	0.732	5.0105	112.1	−0.44 *−0.44*	−0.31 *−0.39*
Cu-Pt	0.806	4.9720	144.2	−0.16	−0.15
	0.830	5.0087	144.4	−0.22 *−0.53*	−0.11 *−0.30*
Ga-In	0.073	5.6081	67.2	0.37	0.66
	0.222	5.8336	37.6	0.26	0.13
In-Mo	2.443	5.6702	104.2	0.88	1.16
	2.280	5.4913	110.7	0.82	1.31
In-Nb	1.237	5.7912	92.1	0.18	0.43
	1.346	5.6362	101.5	0.17	0.36
In-Ni	0.182	5.2340	55.1	−0.23	0.66
	0.298	5.2339	85.2	−0.18	0.26
In-Pd	−0.743	5.4776	83.1	−1.57	−1.59
	−0.570	5.4776	84.9	−1.54	−1.72
In-Pt	−0.570	5.4751	107.7	−0.75	−1.50
	−0.518	5.5008	107.9	−1.22	−1.33
In-Ta	1.577	5.8601	93.0	0.02	0.42
	1.982	5.6114	106.4	0.10	0.15
In-W	3.455	5.7766	120.4	1.07	1.45
	3.440	5.5130	118.7	1.01	1.49

Table 5 Comparison of MEAM-calculated and experimentally determined binding enthalpies for indium with solutes in FCC metals

Host	Solute	MEAM H_B (eV)	Experiment H_B (eV)	Ref.
Ag	Au	0.045	0.025	[30, 31]
	Cu	0.020	0.012	[30]
	Ga	−0.043	−0.113	[30]
	Pd	0.119	0.133	[30]
	Pt	0.147	0.171	[30]
Au	Ag	−0.046	−0.025	[31]
	Pd	0.085	0.13	[29]
	Pt	0.148	0.122	[29]
Cu	Pd	0.123	0.09	[29]
	Pt	0.144	0.062	[29]

Table 6 Comparison of MEAM-calculated and experimentally determined binding enthalpies for indium with vacancies in FCC and BCC metals

Host	MEAM H_B (eV)	Experiment H_B (eV)	Ref.
Al	0.217		
Ag	0.176	0.18	[32]
Au	0.164	0.20	[32]
Cu	0.461	0.24	[32]
Ni	0.565		
Pd	0.139		
Pt	0.468	0.38	[32]
Mo	0.498	0.42	[33, 34]
Nb	0.382	0.31	[33, 35]
Ta	0.326	0.39	[33, 36]
W	0.484	0.71	[33, 37]

Inspection of parameters in Table 4 does not appear to reveal any clues about the origin of these two large deviations. In fact, the target parameters for In-W were matched well by the MEAM calculations.

The binding enthalpies in Tables 5 and 6 are plotted in Fig. 1. In this format, the MEAM results appear to be in good overall agreement with experiment. Even with the relatively large absolute disagreement for In-vacancy binding in Cu and W, one can reasonably expect calculations using this model to identify systems in which In-defect binding is small and likely repulsive such as for In-Ga in Ag and In-Ag in Au, in which systems In-defect binding is small and likely attractive such as the other In-solute combinations, and in which systems In-defect binding is likely large such as all the In-vacancy cases. Such a level of precision is sufficient for predicting new experiments that could be performed to study defect association using PAC.

These results suggest that the approach of using NaCl parameters and dilute solution enthalpies as the basis for developing MEAM potential sets and the use of MEAM more generally as a means to calculate defect properties will be successful in guiding the design of new, informative experiments. Additional calculations are needed, however, for a more exhaustive assessment. As such, work is currently under way to broaden the potential set to include other PAC tracers and a number of compounds with stable intermetallic phases

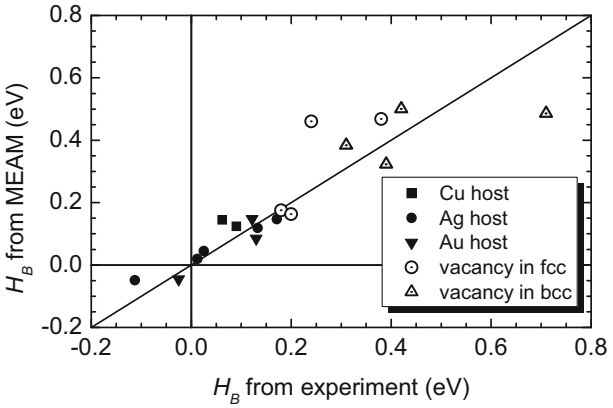

Fig. 1 Comparison of calculated and experimental binding enthalpies. In-solute binding enthalpies in Cu, Ag, and Au are shown as solid symbols. In-vacancy binding enthalpies are shown as open symbols. The line with slope of unity is included to indicate perfect agreement between the model and experiment and is not the result of a linear fit

for which defect formation enthalpies and indium-defect interactions will be calculated and compared against experimental results.

4 Summary

Indium-solute and indium-defect binding enthalpies for selected FCC and BCC metals were calculated and compared to results obtained from perturbed angular correlation spectroscopy. The modified embedded atom method by Baskes and coworkers was used. Parameters of the model were determined using a slight variation from earlier studies. The model was parameterized by considering the formation enthalpies, lattice parameters, and bulk moduli of hypothetical binary alloys with the NaCl structure and by considering dilute solution enthalpies. This parameter set successfully reproduces the binding enthalpies investigated in this study, suggesting that it is worthwhile to explore this simulation method further for its possible broader use in predicting defect properties in other metals and in intermetallic compounds.

Acknowledgment This work is supported in part by NSF grant DMR 15-08189.

Appendix

This section contains details about the embedding function and the short range potential contributions to the total energy in the MEAM as implemented in the present work.

The embedding function for an atom of type i is given by

$$F_i(\bar{\rho}_i) = A_i(E_c)_i \frac{\bar{\rho}_i}{\rho_i^0} \ln\left(\frac{\bar{\rho}_i}{\rho_i^0}\right) \tag{4}$$

where A_i is an adjustable parameter, $(E_c)_i$ is the cohesive energy, and $\bar{\rho}_i^0$ is the background electron density for a given reference structure, taken as the equilibrium structure at ambient conditions as determined from experiment. Note that $F(\bar{\rho}_i = \bar{\rho}_i^0) = 0$.

The background electron density is constructed using the orthogonal partial electron density functions denoted $\rho_i^{(0)}$, $\rho_i^{(1)}$, $\rho_i^{(2)}$ and $\rho_i^{(3)}$, defined as follows [12, 53]:

$$\rho_i^{(0)} = \sum_{j\neq i} \rho_j^{a(0)}(r_{ij}) S_{ij},$$

$$\left(\rho_i^{(1)}\right)^2 = \sum_{\alpha} \left[\sum_{j\neq i} \frac{r_{ij}^{\alpha}}{r_{ij}} \rho_j^{a(1)}\left(r_{ij}\right) S_{ij}\right]^2,$$

$$\left(\rho_i^{(2)}\right)^2 = \sum_{\alpha,\beta} \left[\sum_{j\neq i} \frac{r_{ij}^{\alpha}}{r_{ij}} \frac{r_{ij}^{\beta}}{r_{ij}} \rho_j^{a(2)}\left(r_{ij}\right) S_{ij}\right]^2 - \frac{1}{3}\left[\sum_{j\neq i} \rho_j^{a(2)}(r_{ij}) S_{ij}\right]^2,$$

and

$$\left(\rho_i^{(3)}\right)^2 = \sum_{\alpha,\beta,\gamma} \left[\sum_{j\neq i} \frac{r_{ij}^{\alpha}}{r_{ij}} \frac{r_{ij}^{\beta}}{r_{ij}} \frac{r_{ij}^{\gamma}}{r_{ij}} \rho_j^{a(3)}\left(r_{ij}\right) S_{ij}\right]^2 - \frac{3}{5}\sum_{\alpha}\left[\sum_{j\neq i} \frac{r_{ij}^{\alpha}}{r_{ij}} \rho_j^{a(3)}(r_{ij}) S_{ij}\right]^2.$$

In the above, Greek letters are summation indexes over Cartesian coordinates so that, for example, r_{ij}^{α} denotes the α^{th} Cartesian component of vector $\mathbf{r_{ij}}$ between atoms i and j. The above definitions include what are termed atomic electron densities, defined by

$$\rho_j^{a(h)}\left(r_{ij}\right) = \rho_{j0} \exp\left[-\beta_j^{(h)}\left(r_{ij}/r_{ij}^0 - 1\right)\right] \tag{5}$$

where the $\beta_j^{(h)}$ are four adjustable parameters, r_{ij}^0 denotes the equilibrium atomic separation in the reference structure, and ρ_{j0} is an element-dependent density scaling factor. In a pure metal, total energy calculations are independent of ρ_{j0}; however, interactions between unlike atoms depend on ρ_{j0}.

The above partial electron density functions depend on an atomic screening function S_{ij} that is defined by [54]

$$S_{ij} = f_c\left(\frac{(r_c)_{ij} - r_{ij}}{\Delta r_{ij}}\right) \prod_{k\neq i,j} S_{ijk}$$

where f_c is a radial cutoff function, $(r_c)_{ij}$ is the cutoff separation, Δr_{ij} is the smoothing range of the taper function, k is a product index over yet another atom, and the S_{ijk} are screening factors. The $f_c(x)$ function is defined by

$$f_c[x] \equiv \begin{cases} 1 & 1 \leq x \\ \left[1-(1-x)^4\right]^2 & 0 < x < 1 \\ 0 & x \leq 0 \end{cases}.$$

The screening factors are defined in terms of the same $f_c(x)$ function as

$$S_{ijk} = f_c\left[\frac{C - C_{\min}}{C_{\max} - C_{\min}}\right]$$

where

$$C = \frac{2\left(\frac{r_{ij}}{r_{ik}}\right)^2 + 2\left(\frac{r_{jk}}{r_{ik}}\right)^2 - \left[\left(\frac{r_{ij}}{r_{ik}}\right)^2 - \left(\frac{r_{jk}}{r_{ik}}\right)^2\right]^2 - 1}{1 - \left[\left(\frac{r_{ij}}{r_{ik}}\right)^2 - \left(\frac{r_{jk}}{r_{ik}}\right)^2\right]^2}$$

and the factors $C_{\min}$ and $C_{\max}$ are parameters of the model. C_{max} is usually taken to be 2.8, but C_{min} varies according to the atom types i, j, and k in the interaction.

Baskes and co-workers have used more than one method to calculate the background electron density from the partial densities. In the present work, the form introduced by Ravelo and Baskes [55] is used. It is

$$\bar{\rho}_i = \rho_i^{(0)} G\left(\Gamma_i\right)$$

where

$$G\left(\Gamma_i\right) = \frac{2}{1 + \exp\left(-\Gamma_i\right)}$$

with

$$\Gamma_i = \sum_{h=1}^{3} t_i^{(h)} \left(\frac{\rho_i^{(h)}}{\rho_i^{(0)}}\right)^2 \tag{6}$$

and $t_i^{(h)}$ are 3 more adjustable parameters.

The short range potential $\phi\left(r_{ij}\right)$ is defined to be the difference between the energy contribution of the embedding function $F_i\left(\bar{\rho}_i\right)$ and the total energy given by $E_{\text{Rose}}\left(r_{ij}\right)$, which is Rose's universal equation of state [56], parameterized here by the nearest neighbor distance between atoms i and j in the structure of interest:

$$E_{\text{Rose}}\left(r_{ij}\right) = -\left(E_c\right)_{ij}\left(1 + a_{ij}^* + d_{ij}\left(a_{ij}^*\right)^3\right)\exp\left(-a_{ij}^*\right) \tag{7}$$

where $a_{ij}^* = \alpha_{ij}\left(r_{ij}/r_{ij}^0 - 1\right)$ with $\alpha_{ij} = \left(9B_{ij}\Omega_{ij}/\left(E_c\right)_{ij}\right)^{1/2}$, d_{ij} is an adjustable parameter, and the remaining parameters $\left(E_c\right)_{ij}$, B_{ij}, and Ω_{ij} are the cohesive energy, bulk modulus and atomic volume of the reference structure used to parameterize atoms i and j. The method used to calculate $\phi\left(r_{ij}\right)$ when screening factors allow second neighbor interactions to be included in the embedding function is described in Ref. [13].

References

1. Zacate, M.O., Favrot, A., Collins, G.S.: Atom movement in In_3La studied via nuclear quadrupole relaxation. Phys. Rev. Lett. **92**, 225901 (2004); Erratum, Phys. Rev. Lett. **93**, 49903 (2004)
2. Collins, G.S., Jiang, X., Bevington, J.P., Selim, F., Zacate, M.O.: Change of diffusion mechanism with lattice parameter in the series of lanthanide indides having $L1_2$ structure. Phys. Rev. Lett. **102**, 155901 (2009)
3. Lockwood, M., Norman, B., Newhouse, R., Collins, G.S.: Comparison of jump frequencies of ^{111}In/Cd tracer atoms in Sn_3R and In_3R phases having the $L1_2$ structure (R= rare earth). Defect Diffus. Forum **311**, 159–166 (2011)
4. Jiang, X., Zacate, M.O., Collins, G.S.: Jump frequencies of Cd tracer atoms in $L1_2$ lanthanide gallides. Defect Diffus. Forum **725**, 289–292 (2009)
5. Wang, Q., Collins, G.S.: Nuclear quadrupole interactions of ^{111}In/Cd solute atoms in a series of rare-earth palladium alloys. Hyperfine Interact. **221**, 85–98 (2013)
6. Zacate, M.O., Collins, G.S.: Jump Frequency of Cd tracer atoms in β-Mn. Defect Diffus. Forum **237-240**, 396–401 (2005)

7. Nieuwenhuis, E.R., Zacate, M.O., Collins, G.S.: Simultaneous measurement of tracer jump frequencies on different sublattices in Ga_7Pd_3 using PAC. Defect Diffus. Forum **264**, 27–32 (2007)
8. Selim, F., Bevington, J.P., Collins, G.S.: Diffusion of ^{111}Cd probes in Ga_7Pt_3 studied via nuclear quadrupole relaxation. Hyperfine Interact. **178**, 87–90 (2008)
9. Newhouse, R., Collins, G.S.: Diffusion in La_nCoIn_{3n+2} phases studied by perturbed angular correlation. Diffus. Defect Data, Pt. A **323–325**, 453–458 (2012)
10. Lage, S., Collins, G.S.: Motion of cadmium tracer atoms in $Al_{11}R_3$ phases (R=La, Ce, Pr). Diffus. Defect Data, Pt. A **289–292**, 755–761 (2009)
11. Newhouse, R., Collins, G.S., Zacate, M.O.: Site occupation of indium and jump frequencies of cadmium in $FeGa_3$. Submitted to Hyperfine Interactions for publication in the same volume
12. Baskes, M.I.: Modified embedded-atom potentials for cubic materials and impurities. Phys. Rev. B **46**, 2727–2742 (1992)
13. Lee, B.-J., Baskes, M.I., Kim, H., Cho, Y.K.: Second nearest-neighbor modified embedded atom method potentials for BCC transition metals. Phys. Rev. B **64**, 184102 (2001)
14. Lee, B.-J., Shim, J.-H., Baskes, M.I.: Semiempirical atomic potentials for the FCC metals Cu, Ag, Au, Ni, Pd, Pt, Al and Pb based on first and second nearest-neighbor modified embedded atom method. Phys. Rev. B **68**, 144112 (2003)
15. Baskes, M.I., Chen, S.P., Cherne, F.J.: Atomistic model of gallium. Phys. Rev. B **66**, 104107 (2002)
16. Kim, Y.-M., Lee, B.-J., Baskes, M.I.: Modified embedded-atom method interatomic potentials for Ti and Zr. Phys. Rev. B **74**, 014101 (2006)
17. Kim, Y.-M., Kim, N.J., Lee, B.-J.: Atomistic modeling of pure Mg and Mg-Al systems. CALPHAD: Comput. Coupling Phase Diagrams Thermochem. **33**, 650–657 (2009)
18. Do, E.C., Shin, Y.-H., Lee, B.-J.: A modified embedded-atom method interatomic potential for indium. Comput. Coupling Phase Diagrams Thermochem. **32**, 82–88 (2008)
19. Lee, B.-J.: A modified embedded atom method interatomic potential for silicon. Calphad **31**, 95 (2007)
20. Do, E.C., Shin, Y.-H., Lee, B.-J.: A modified embedded-atom method interatomic potential for indium. Comput. Coupling Phase Diagrams Thermochem. **32**, 82–88 (2008)
21. Baskes, I.M., Angelo, J.E., Bisson, C.L.: Atomistic calculations of composite interfaces. Phys. Rev. B **46**, 2727 (1992)
22. Jelinek, B., Groh, S., Horstemeyer, M.F., Houze, J., Kim, S.G., Wagner, G.J., Moitra, A., Baskes, M.I.: Modified embedded atom method potential for Al, Si, Mg, Cu, and Fe alloys. Phys. Rev. B **85**, 245102 (2012)
23. Baskes, M.I.: Atomistic potentials for the molybdenum-silicon system. Mater. Sci. Eng. A **261**, 165–168 (1999)
24. Do, E.C., Shin, Y.-H., Lee, B.-J.: Atomistic modeling of III-V nitrides: modified embedded-atom method interatomic potentials for GaN, InN, and $Ga_{1-x}In_xN$. J. Phys.: Condens. Matter **21**, 325801 (2009)
25. Gall, K., Horstemeyer, M.F., van Schilfgaarde, M., Baskes, M.I.: Atomistic simulations on the tensile debonding of an aluminum–silicon interface. J. Mech. Phys. Solids **48**, 2183 (2000)
26. Huang, H., Ghoniem, N.M., Wong, J.K., Baskes, M.I.: Molecular dynamics determination of defect energetics in β-SiC using three representative empirical potentials. Modell. Simul. Mater. Sci. Eng. **3**, 615–627 (1995)
27. Lee, B.-J., Ko, W.-S., Kim, H.-K., Kim, E.-H.: The modified embedded-atom method interatomic potentials and recent progress in atomistic simulations. CALPHAD: Comput. Coupling Phase Diagrams Thermochem. **34**, 510–522 (2010)
28. Jelinek, B., Groh, S., Horstemeyer, M.F., Houze, J., Kim, S.G., Wagner, G.J., Moitra, A., Baskes, M.I.: Modified embedded atom method potential for Al, Si, Mg, Cu, and Fe alloys. Phys. Rev. B **85**, 245102 (2012)
29. Baumvol, I.J.R., Behar, M., Da Jornada, J.A.H., Livi, R.P., Lodge, K.W., Lopez Garcia, A., Zawislak, F.C.: Electric field gradients and impurity distributions in doped noble metals: a systematic study. Phys. Rev. B **22**, 5115–5127 (1980)
30. Królas, R.: Impurity-impurity interactions in dilute alloys. Hyperfine Interact. **60**, 581–597 (1990)
31. Butt, R., Haas, H., Rinneberg, H.: Nearest neighbor contribution to the electric field gradient at Cd in silver-gold alloys. Phys. Lett. A **60**, 323 (1977)
32. Pleiter, F., Hohenemser, C.: Interpretation of vacancy migration, trapping, and clustering in fcc metals as observed through perturbed angular correlations and distributions of γ rays. Phys. Rev. B **25**, 106 (1982)
33. Collins, G.S., Zacate, M.O.: Charge transfer model for quadrupole interactions and binding energies of point defects with ^{111}In/Cd probes in cubic metals. Hyperfine Interact. **151/152**, 77–91 (2003)
34. Weidinger, Al., Wessner, R., Recknagel, E., Wichert, Th.: Annealing behaviour of particle irradiated molybdenum foils. Nucl. Instr. Meth. **182/183**, 509 (1981)

35. Sielemann, R., Metzner, H., Butt, R., Klaumuenzer, S., Hass, H., Vogl, G.: Free migration of vacancies in niobium at 250 K. Phys. Rev. B **25**, 5555 (1982)
36. Sielemann, R., Metzner, H., Hunger, E., Klaumuenzer, S.: Migration of vacancies in tantalum and stage III recovery in refractory BCC metals observed by PAC. Phys. Lett. A **117**, 86 (1986)
37. Van der Kolk, G.J., Post, K., van Veen, A., Pleiter, F., do Hosson, J.Th.M.: Interaction of vacancies with implanted metal atoms in tungsten observed by means of thermal helium desorption spectrometry and perturbed angular correlation measurements. Radiat. Eff. **84**, 131 (1985)
38. Daw, M.S., Baskes, M.I.: Embedded-atom method: Derivation and application to impurities, surfaces, and other defects in metals. Phys. Rev. B **29**, 6443–6453 (1984)
39. Daw, M.S., Baskes, M.I.: Semiempirical, quantum mechanical calculation of hydrogen embrittlement in metals. Phys. Rev. Lett. **50**, 1285–8 (1983)
40. Gale, J.D.: GULP - a computer program for the symmetry adapted simulation of solids. JCS Faraday Trans. **93**, 629 (1997)
41. Gale, J.D., Rohl, A.L.: The general utility lattice program. Mol. Simul. **29**, 291–341 (2003)
42. Blöchl, P.E.: Projector augmented-wave method. Phys. Rev. B **50**, 17953 (1994)
43. Kresse, G., Joubert, J.: From ultrasoft pseudopotentials to the projector augmented wave method. Phys. Rev. B **59**, 1758 (1999)
44. Kresse, G., Hafner, J.: Ab initio molecular dynamics for liquid metals. Phys. Rev. B **47**, 558 (1993)
45. Kresse, G., Furthmüller, J.: Efficient iterative schemes for ab initio total-energy calculations using a plane-wave basis set. Phys. Rev. B **54**, 11169 (1996)
46. Perdew, J.P., Chevary, J.A., Vosko, S.H., Jackson, K.A., Pederson, M.R., Singh, D.J., Fiolhais, C.: Atoms, molecules, solids, and surfaces: Applications of the generalized gradient approximation for exchange and correlation. Phys. Rev. B **46**, 6671 (1992)
47. Monkhorst, H.J., Pack, J.D.: Special points for Brillouin-zone integrations. Phys. Rev. B **13**, 5188 (1976)
48. Birch, F.: Finite elastic strain of cubic crystals. Phys. Rev. **71**, 809–824 (1947)
49. deBoer, F.R., Boom, R., Mattens, W.C.M., Miedema, A.R., Niessen, A.K.: Cohesion in Metals – Transition Metal Alloys. North Holland (1988)
50. Bakker, H., Woehlbeir, F.H.: Enthalpies in Alloys – Miedema's Semi-Empirical Model, Materials Science Foundations. In: Magini, M. (ed.) vol. 1. Trans. Tech. Publications, Ltd, Switzerland (1998)
51. Eshelby, J.D.: The continuum theory of lattice defects. In: Seitz, F., Turnbull, D. (eds.) Solid State Physics, vol. 3. Academic Press, New York (1956)
52. Hultgren, R., Desai, P.D., Hawkins, D.T., Gleiser, M., Kelley, K.K.: Selected Values of the Thermodynamic Properties of Binary Alloys. American Society for Metals, Metals Park, OH (1973)
53. Baskes, M.I.: Atomistic potentials for the molybdenum-silicon system. Mater. Sci. Eng. A **261**, 165–168 (1999)
54. Baskes, M.I.: Determination of modified embedded atom method parameters for nickel. Mater. Chem. Phys. **50**, 152–158 (1997)
55. Ravelo, R.J., Baskes, M.I.: Free energy calculations of Cu-Sn interfaces. In: Materials Research Society Symposium - Proceedings, pp. 287–293. Materials Research Society, Pittsburgh (1996)
56. Rose, J.H., Smith, J.R., Guinea, F., Ferrante, J.: Universal features of the equation of state of metals. Phys. Rev. B **29**, 2963 (1984)